Synaptic inhibition in the accessory olfactory bulb regulates pheromone location learning and memory

Shruti D. Marathe[1], and Nixon M. Abraham[1,*]

[1] Laboratory of Neural Circuits and Behaviour (LNCB), Department of Biology, Indian Institute of Science Education and Research (IISER), Pune, Maharashtra, 411008, India.

* Correspondence: nabraham@iiserpune.ac.in

Running title: Neural mechanisms of pheromone location learning

Number of Figures: 5

Correspondence:
Dr. Nixon M. Abraham
Laboratory of Neural Circuits and Behaviour (LNCB)
Department of Biology
Indian Institute of Science Education and Research (IISER), Pune
Maharashtra, India. 411008
Email: nabraham@iiserpune.ac.in
Phone: 0091 20 25908283

Abstract:

Pheromone signaling is pivotal in driving social and reproductive behaviors of rodents. Learning and memorizing the pheromone locations involve olfactory subsystems. To study the neural basis of this behavior, we trained female heterozygous knockouts of GluA2 (AMPAR subunit) and NR1 (NMDAR subunit), targeting GAD65 interneuron population, in a pheromone place preference learning assay. We observed memory loss of pheromone locations on early and late recall periods, pointing towards the possible role of ionotropic glutamate receptors (iGluRs), and thereby the synaptic inhibition in pheromone location learning. Correlated changes were observed in the expression levels of activity-regulated cytoskeletal (*Arc)* protein, which is critical for memory consolidation, in the associated brain areas. Further, to probe the involvement of main olfactory bulb (MOB) and accessory olfactory bulb (AOB) in pheromone location learning, we knocked out NR1 and GluA2 from MOB and/or AOB neuronal circuits by stereotaxic injection of Cre-dependent AAV5 viral particles. Perturbing the inhibitory circuits of MOB and AOB & AOB-alone resulted in the loss of pheromone location memory. These results confirm the role of iGluRs and the synaptic inhibition exerted by the interneuron network of AOB in regulating learning and memory of pheromone locations.

Introduction

The vomeronasal system, one of the subsystems of rodent olfactory system, plays a critical role in pheromone information processing (Halpern, 1987; Wyatt, 2014). The neuronal circuitry starting at the vomeronasal organ (VNO), and passing through the accessory olfactory bulb, vomeronasal amygdala, and the preoptic area of hypothalamus, is involved in this process, which is vital for the survival of animals (Lehman et al., 1980; Dulac and Torello, 2003; Isogai et al., 2011; Li et al., 2017; Tirindelli, 2021). While the terrestrial rodents encounter the pheromones streaked on objects of different shapes and sizes, their whisker system is getting involved in sampling the features of objects. This multimodal association in pheromone location learning has been proven previously (Pardasani et al., 2021). Here we addressed the neural mechanisms of pheromone location learning and memory by focusing on the main and accessory olfactory bulb (MOB & AOB) neuronal circuits.

Male mice mark their territories through urine depositions in many social contexts (Arakawa et al., 2008). It has been found that non-volatile components of mouse urinary pheromones are processed by the MOB circuits and the volatile components by the AOB circuits. While the VNO type 1, type 2, and formyl peptide receptors sense the non-volatile components, trace amine-associated receptors expressed on the main olfactory epithelium are activated by the volatile pheromones (Dulac and Torello, 2003; Liberles and Buck, 2006; Holy, 2018; Murata and Touhara, 2021). This information is further received and processed at the AOB and MOB by the projection neurons (Mombaerts et al., 1996; Mombaerts, 2004). The inhibitory network of MOB and AOB, which forms dendrodendritic synapses with the projection neurons refine the odorant/pheromone information before being conveyed to the higher centers (Aungst et al., 2003; Abraham et al., 2010; Maksimova et al., 2019; Pardasani et al., 2023).

The vomeronasal sensory neurons (VSNs) expressing the same vomeronasal receptors project to multiple glomeruli in the AOB. This organization is different from that of MOB (Belluscio et al., 1999; Rodriguez et al., 1999; Del Punta et al., 2002). Unlike in MOB, the projection neuron cell bodies are dispersed in AOB, and their primary dendrites target multiple glomeruli (Dulac and Wagner, 2006; Salazar et al., 2006). AOB projection neurons have been shown to be selective for the sex of urine donor, and the inhibitory network is critical in shaping this selectivity (Luo et al., 2003; Hendrickson et al., 2008). The inhibitory network of AOB is constituted by the GABAergic periglomerular interneurons and granule cells (GCs) (Hayashi et al., 1993; Taniguchi and Kaba, 2001). There are several morphologically and physiologically distinct classes of interneurons in the AOB. Among these, GAD65-expressing ones represent a significant population (Maksimova et al., 2019). The projection neurons release glutamate, which activates ionotropic glutamate receptors (iGluRs) on GCs, and in response they release GABA, which causes the inhibitory feedback on the projection neurons (Mohrhardt et al., 2018).

To probe the neural mechanisms of pheromone location learning, we modulated the functioning of MOB and AOB inhibitory network by targeting iGluRs expressed on GAD65 inhibitory interneurons (Mahajan et al., 2024). After the conditional deletion of GluA2 subunit of AMPARs, and NR1 subunit of NMDARs, we trained female heterozygous knockouts (KOs) of GluA2 and NR1, in a pheromone place preference learning assay. We observed the loss of memory towards pheromone locations on early and late recall periods, pointing towards the possible role of iGluRs and thereby the synaptic inhibition in pheromone location learning and memory. Correlated changes were observed in the expression levels of activity-regulated cytoskeletal (*Arc)* protein, which is critical for memory consolidation, in the associated brain areas. To study the involvement of MOB and AOB microcircuitry in multimodal learning of pheromone locations, we specifically knocked out NR1 and GluA2 from MOB and/or AOB neuronal circuits by injecting Cre-dependent AAV5 viral particles stereotaxically. Perturbing the neuronal circuitry of MOB and AOB or AOB-alone resulted in the loss of pheromone location memory.

These results confirm the role of iGluRs and the synaptic inhibition exerted by the interneuron network of AOB in controlling the learning and memory of pheromone locations.

Materials and Methods

Animals

A total of 37 control C57BL/6J female mice, aged 8-12 weeks, were utilized for these experiments (experiment wise breakup of animals is mentioned in the corresponding data). In addition to the wild type animals, transgenic mice were obtained by crossing the following genotypes that were obtained from The Jackson's laboratory, unless mentioned otherwise.

GluA2^{2Lox}: GluA2^{2Lox} (Gria2) was obtained from the Heidelberg University, Germany
GluA2$^{GAD65(+/-)}$ knockout: GluA2^{2Lox} with B6N.Cg-Gad2$^{tm2(cre)Zjh}$/J for the knockout of GluA2 in GAD65+ve neurons.
NR1^{2LOX}: NR1^{2Lox} (GRIN1) was obtained from the Heidelberg University, Germany
NR1$^{GAD65(+/-)}$ knockout: NR1^{2Lox} with B6N.Cg-Gad2$^{tm2(cre)Zjh}$/J for the knockout of NR1 in GAD65+ve neurons.
GAD65-GCaMP6f: B6N.Cg-Gad2$^{tm2(cre)Zjh}$/J with B6;129S-Gt(ROSA)26Sor$^{tm95.1(CAGGCaMP6f)Hze}$/J for the expression of GCaMP6f in GAD65+ve cells.

A total of 40 NR1$^{GAD65(+/-)}$ and 28 GluA2$^{GAD65(+/-)}$ female mice aged 8 to 12 weeks old were used for this study. 18 male mice (non-littermates GluA2Lox, NR1Lox) aged 10 to 16 weeks old were used to collect urine and soiled bedding. Control mice included GluA2Lox/NR1Lox.

Ethical Approval

The experimental procedures used in this manuscript are approved by the Institutional Animal Ethics Committee (IAEC) at IISER Pune, and the Committee for the Control and Supervision of Experiments on Animals (CCSEA), Government of India (animal facility CCSEA registration number 1496/GO/ReBi/S/11/CCSEA). The usage of animals in this manuscript was approved under protocol number IISER_Pune/IAEC/2016_01/001.

Calcium Imaging

Calcium imaging was performed as explained previously (Pardasani et al., 2023; Mahajan et al., 2024). In brief, for calcium imaging 5 naïve adult females, 8 to 12 weeks of age were used. The animals were anaesthetized with a mixture of ketamine and xylazine and 1mm diameter cranial window was created at the posterior end of the right hemisphere of the OB using a dental drill. As a precaution, a blunt Hamilton needle was lowered 1.5 mm ventral to the dura in the AOB and kept for 5 minutes to create a path before insertion of the GRIN lens. The 1.5 mm protruding GRIN lens was lowered vertically until it reached the AOB. To stabilize the lens assembly to the skull surface, a mixture of cyanoacrylate gum and acrylic dental cement was used. A headpost was implanted behind the implanted lens and animals were given a month to recover. Ca^{2+} imaging was performed under anesthetized conditions. Firstly, the activity of GAD65 interneurons were investigated under 0.4LPM airflow condition for 40 trials. Next day, the Ca^{2+} activity against male urine was observed for 40-trials. Further, the analysis was done using custom-written Python scripts. A heatmap and selected individual traces were plotted along with average plots for $\Delta F/F$.

Genotyping

NR1Lox and GluA2Lox mice were crossed with GAD65-Cre mice to produce NR1$^{GAD65(+/-)}$ and GluA2$^{GAD65(+/-)}$ heterozygous knockout (KO) animals. Tail samples of the F1 generation males and females were collected and DNA was isolated using a KAPA DNA extraction kit according to manufacturer's instructions. DNA concentration and quality were checked using NanoDrop (Thermo

Fisher Scientific). 50 – 70 μg DNA was used for Polymerase Chain Reaction (PCR). The sequence of primers and thermocycler conditions were as follows:

Name	Primers	PCR Cycling conditions
GAD65-Cre	5'-CACTGCATTCTAGTTGTGGTTTG-3' (Mutant forward) 5'-TCGTTGCACTGACGTGTTCT-3' (Wild type forward) 5'-AACAGTTTGATGAGTGAGGTGA-3' (Common)	Initial denaturation: 94^{0}C, 2 minutes Denaturation: 94^{0}C 20 seconds Annealing temp: 65^{0}C (-0.5^{0}C per cycle), 15 seconds, Extension: 68^{0}C, 10 seconds 10x Denaturation: 94^{0}C, 15 seconds Annealing temp: 60^{0}C 15 seconds, Extension: 72^{0}C, 10 seconds 28x Final extension: 72^{0}C, 2 minutes
NR1^{2Lox}	P1: N1Ex18do1: 5'-CTGGGACTCAGCTGTGCTGG-3' P1b: NR1.2: 5'-CTCAAGTGAGTCTGCCCCATGCTG-3' P2: N1In18up1: 5'-AGGGGAGGCAACACTGTGGAC-3' P2b:NR1.3as: 5'-CACAGGGGAGGCAACACTGTGGAC-3'	Initial denaturation: 94^{0}C, 2 minutes Denaturation: 94^{0}C, 30 seconds Annealing temp: 62.4^{0}C, 30 seconds, Extension: 72^{0}C, 50 seconds 35x Final extension: 72^{0}C, 2 minutes
GluA2^{2Lox}	VM10: 5'-GTTGTCTAACAAGTTGTTGACC-3' VM12: 5'-GCGTAAGCCTGTGAAATACCTG-3' VM17: 5'-GAATCATTGTTGACAGATTGCCAC-3'	Initial denaturation: 94^{0}C, 2 minutes Denaturation: 94^{0}C, 30 seconds Annealing temp: 54.4^{0}C, 30 seconds, Extension: 72^{0}C, 50 seconds 35x Final extension: 72^{0}C, 2 minutes

Protein quantification

To quantify the drop in the protein levels of NR1 and GluA2, western blotting was performed. The following groups of animals were used for western blotting: control (NR1^{2Lox}, GluA2^{2Lox}), NR1$^{GAD65(+/-)}$, and GluA2$^{GAD65(+/-)}$ animals [n (number of animals) = 3 each, N (number of replicates) = 2]. Animals aged 6 to 10 weeks were utilized. The animals were anaesthetized in a CO_2 chamber and then decapitated. Both OBs were dissected and immediately flash-frozen. The samples were kept at -80^{0}C until further use. OB lysates were prepared in RIPA buffer (50 mM Tris HCl, pH 7.4, 150 mM NaCl, 1% Triton X-100, 0.5% Sodium deoxycholate, 0.1% SDS, 1 mM EDTA, 10 mM NaF), supplemented with a complete protease inhibitor (Roche Cat # 04693116001). The BCA assay was performed to quantify the total protein concentration using a Pierce BCA protein assay kit (Thermofisher Cat # 23225). Approximately, 20 μg of protein from each sample was loaded onto a 12% SDS-Polyacrylamide Gel Electrophoresis (SDS-PAGE). After separating the proteins based on size, the proteins were transferred to the Immobilon-P PVDF membranes (Millipore Cat # IPVH00010) through methanol buffer transfer. Blocking was carried out with 5% milk/Tris Buffer Saline (TBS)-Tween 20 for 1 hour at room temperature. The membranes were probed with primary antibodies: anti-NR1 antibody (Millipore Cat # AB9864R), anti-GluA2 antibody (Millipore Cat # AB1786-I), and anti-GAPDH (Sigma Cat # G9545) at 1:1000, 1:250 and 1:5000 dilutions, respectively, for approximately 20 hours at 4^{0}C. The blots were washed with 0.1% TBST three times for 15 minutes each. The appropriate secondary antibody used was peroxidase-conjugated AffiniPure Goat anti-rabbit IgG (Jackson ImmunoResearch Cat # 111-035-003), diluted at 1:5000 for 1 hour at room temperature. The bound antibodies were detected using Clarity ECL Western Blotting Substrate (BioRad Cat # 1705061), with the image digitally captured using an ImageQuant LAS 4000.

Multimodal Pheromonal location learning apparatus

The multimodal pheromonal location learning apparatus (Fig. 1 A2) has the following dimensions: 60 cm * 30 cm * 15 cm (L * W * H). It was made from a plexiglass and was coated with non-reflective black paint. The setup was divided into three equally sized zones. Zone 1 and Zone 3 had one chamber each of 10 cm * 10 cm * 15 cm (L*W*H) dimension. Zone 1 and Zone 3 were opposite to each other. Each chamber had a removable plate. One pair of plates had 10 mm holes which were equidistant to each other while another pair of plates had 5 mm equidistant holes on it. One pair containing one 10 mm hole-sized plate and one 5 mm hole-sized plate were dedicated to the male urine chamber (marked on top) while the other set was used only for the water chamber. The other three sides of these chambers were without any holes and were fixed. This is to avoid animals sniffing odors from other sides of the chamber and could only get access to odors from the front end of the chamber. Each chamber had a 55 mm petri dish kept inside it. The petri dish kept in the urine chamber contained fresh 100 μl male urine (opposite sex pheromone in chamber 1) while the water chamber had 100 μl of distilled water (neutral stimulus in chamber 2). Two different identical setups were used to carry out training sessions and memory sessions respectively (Pardasani et al., 2021).

Multimodal Pheromone Location Learning Paradigm

The pheromone location learning and memory assay was carried out as explained previously (Pardasani et al., 2021). The assay consists of three phases: 1) the Testing Days phase (TDs), 2) the Training Days phase (TrPs) and 3) Memory Day (MD). The TD was performed for an initial four days. During TDs female mouse was allowed to roam in the setup unrestricted for 10 mins and the activity was video recorded. The TD is done to check if any female has an innate preference towards the male urine chamber over the water chamber. The setup was rotated by 180^0 every day to avoid any bias towards spatial location throughout the TDs and TrDs. During TD, male urine (MU) and water (NS) are kept in the respective chambers. Soiled bedding (SB) from the male cage from which urine has collected is also spread at the front of the male urine chamber. This ensures volatiles as well as non-volatiles are emanating from the male pheromones.

During each experiment, female mice were counterbalanced towards a particular hole size on the plate (e.g., half female mice had a 10 mm hole-sized plate in the urine chamber and a 5 mm hole-sized plate in the water chamber. For the rest of the females, the urine chamber had a 5 mm hole-sized plate and the water chamber had a 10 mm hole-sized plate). This counterbalancing was done to avoid any predisposition of female mice towards a particular hole size.

TrDs were conducted for the next 15 days. During TrDs, the female animal was confined to both zones for 15 minutes each, alternating after every 5 minutes in Zone 1 and 3. This was continued for 30 minutes every day for 15 days). Every day the setup was rotated by 180^0. During each training day fresh MU, MB and water were used. Memory was tested on a different setup which was identical to the training setup. This was done to avoid animals sensing any remnant cues in the setup.

Behavior quantification

Two parameters were quantified in pheromone place assay, 1) 'Time spent' near Zone 1 vs Zone 2, and 2) 'number of active attempts' done towards respective plates. EthoVision software (Noldus Information Technology, version 8.5 XT) was used for quantifying 'time spent'. The nose point feature was used for the quantification. The number of active attempts suggested nose pokes done by the animal. Active attempts were counted manually.

Immunohistochemistry

After memory testing days 7 and 15, animals were sacrificed and trans-cardially perfused with 1X PBS and 4% paraformaldehyde within 30 minutes of an experiment to quantify the expression of Activity-regulated cytoskeletal (Arc) in the olfactory bulb (main and accessory olfactory bulb), hippocampus and somatosensory cortex (SSC). Brains were kept in 4% PFA overnight at 4^0C. A brief wash with 1X

PBS was given and the brains were transferred to 30% sucrose which acted as a cryoprotectant. Once the brains submerged in the sucrose solution, they were embedded in a block using freezing media. 50 μm thick coronal sections were cut using a cryotome. We selected every 6th section of OB, hippocampus and SSC for staining purposes. The sections were washed with 1% triton in 1X PBS for 10 mins. Then the sections were incubated in a blocking buffer (5% BSA in 0.5% triton and 1X PBS) for 1.5 hours at room temperature. Primary antibody incubation (1:750 μl of anti-Rabbit Arc antibody in 0.5% BSA in 0.1% triton and 1X PBS) was done overnight at 4^0C. Three washes with 1X PBS were done for 15 minutes each. During the last wash DAPI (4',6'-diamidino-2-phenylindole) was added to visualize nuclei under the microscope. Secondary antibody incubation (anti-Rabbit Alexa-fluor 488 1:1000) was done for 2 hours at room temperature. Three washes with 1X PBS were done for 10 mins each. The sections were mounted on slides and were light-protected with a Vectashield. The sections were imaged using a Leica SP8 confocal fluorescent upright microscope. Imaging was done under 20X.

Confocal imaging and cell count quantification

c-Fos and Arc expressing cells across OB, AOB, hippocampus and SSC were imaged using a Leica SP8 confocal microscope. 4 to 6 sections per brain area per mouse were used for quantification. The cell quantification was done using Imarisx64 software (Bitplane, Oxford Instruments). For quantification, each section with a Z-stack of 1 μm step size was used. To reduce the background noise, A constant Gaussian filter was applied to every stack. The threshold used to count the c-Fos and Arc-expressing cells was automatically set by the software Imaris. False positive counts were removed manually. The total cells counted for each brain region was equal to the sum of the cells counted per stack. The total volume was obtained by multiplying the thickness of the stack with the XY diameter of the image. The final number of c-Fos and Arc positive cells counted was per 1 mm^3.

Stereotaxic surgeries

Female mice aged 6 to 8 weeks were injected with Cre-viral particles (pAAV.CMV.HI.eGFP-Cre.WPRE.SV40), using a BENCHMARKTM stereotaxic instrument (myNeurolab, St. Louis, MO) and LEICA MZ6 stereo microscope (Leica Microsystems, Germany). MOB- specific injection were done as described previously (Abraham et al., 2010). AOB-specific injection coordinates were decided based on the previous reports (Kang et al., 2009). In brief, the optimization of injection coordinates was done after few fluorescent dye injections. Injection pipette tip was positioned at the bregma and all axes were set to zero. The pipette tip was then was moved to the anterior side near the intersection of sagittal suture and infra-cerebral vein, where the Z coordinate was adjusted according to the Z coordinate at bregma. The coordinates were made zero across the three axes. Based on this local reference point, injection coordinates were decided. A total of two injections were done in each bulb. A resting period on 5 – 7 mins was given after each injection to avoid backflow of the viral particles. At each spot, around 100 – 150 nl of solution was injected. The animals were allowed to recover for the next three weeks before starting with the behavioural experiment.

Data and Statistical analysis

GraphPad Prism 9, Microsoft Excel, and Python were used for all statistical analyses in this study. The data is presented as Mean ± SEM. To determine p-values and test for statistical significance, we used the student's t-test, one-way and two-way ANOVA, and associated post-hoc tests.

Results:

Main and accessory olfactory bulb inhibitory networks are involved in pheromone location learning

Learning and memorizing the information of pheromone locations is critical for the reproductive success and survival of animals. To study the pheromone location learning abilities of mice, we

developed a pheromonal place preference assay as described before (Pardasani et al., 2021). We trained a batch of wild type mice to associate specific hole sizes with zones containing opposite sex urine vs. neutral stimulus (Figure 1 A). After 15 days of training, their memory was tested in the absence of these stimuli. Whisker-intact mice showed memory of the pheromone location, quantified by the time spent in front of the pheromone chamber and number of active attempts made by the animals to sample, compared to the chamber containing neutral stimulus, water (Figure 1B1,B2, paired two-tailed student's t-test, n = 6 females). Whisker deprivation caused the inability to learn such pheromone locations (Figure 1C1,C2, paired two-tailed student's t-test, n = 6).

To investigate the role of olfactory bulb circuits in such a learning, mice were sacrificed immediately after the training was completed and the c-Fos (a neuronal activity marker) expression pattern was studied. We observed many activated cells among the interneuron layers in MOB and AOB, indicating the plausible involvement of interneuron network in pheromone location learning (Figure 1D1-D3). To confirm the involvement of inhibitory network in processing pheromonal cues, we expressed GCaMP6f in GAD65-expressing interneurons, which comprise the majority of interneurons in MOB and AOB. The calcium activity was monitored using a GRIN lens implanted in the AOB of GAD65-GCaMP6f transgenic female mice in response to male urinary volatiles (Figure 1D4,D5). As a control, calcium activity was recorded in response to airflow (0.4 LPM). This population activity was measured under anaesthesia. The fluorescence change ($\Delta F/F_0$) was quantified for 40 trials across 5 female mice (Figure 1E). We observed significantly higher responses towards urinary volatiles compared to airflow stimuli in all animals, confirming the activation of inhibitory network (Figure 1E1-E5).

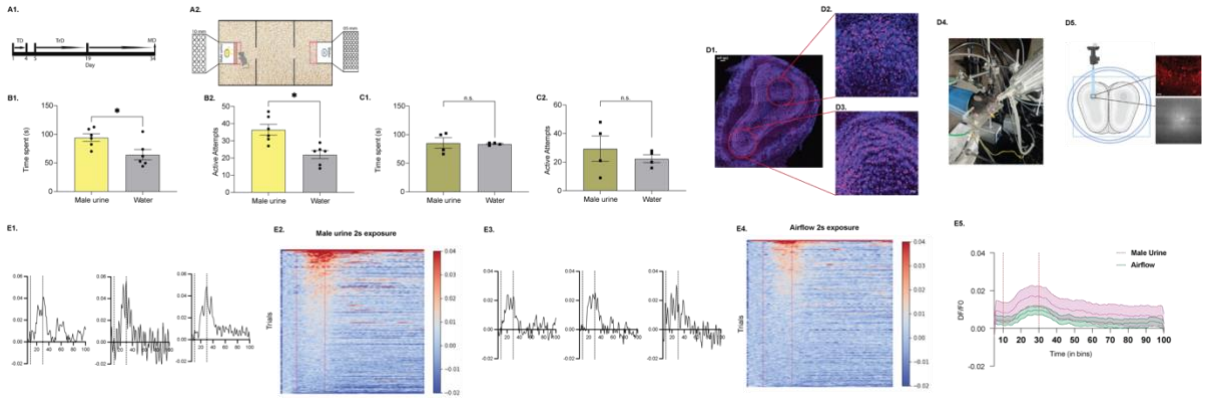

Figure 1: Inhibitory network of main and accessory olfactory bulbs are involved in pheromone location learning

A: A1 Timeline of pheromone location learning assay, A2 Diagrammatic representation of pheromone location learning setup. B: Whisker-intact females spent significantly longer time near to male urine chamber compared to neutral stimulus chamber (B1, p = 0.0312, paired two-tailed student's t-test, N = 6 females), and made significantly higher number of active attempts to sample (B2, p = 0.0312, paired two-tailed student's t-test, N = 6 females) on memory testing day, MD 15. C: C1. Whisker-deprived females showed similar time spent on both zones on MD 15 (p = 0.3750, paired two-tailed student's t-test, N = 4 females). C2. Whisker-deprived females displayed a similar number of active attempts for both zones on MD 15 (p = 0.5, paired two-tailed student's t-test, N = 4 females). D: D1. Coronal section of mouse OB showing c-Fos expression (magenta) across various layers of OB. The magnified image shows C-Fos expression upon pheromone expression in AOB (DAPI shown in blue). D2. Experimental setup to record Ca^{2+} dynamics under anesthetized conditions. D3. Illustration representing micro-endoscopic calcium imaging in the accessory olfactory bulb. E: E1. Examples of Ca^{2+} responses of GAD65-expressing interneurons to a male urine exposure under anesthetized conditions. E2. Pseudo-coloured heatmap showing Ca^{2+} responses in the GAD65-expressing interneurons of AOB, in response to male urine exposure for 2 seconds (red lines) in a female mouse. E2. Examples of Ca^{2+} responses of

GAD65-expressing interneurons to a male urine exposure under anesthetized conditions. E3. Examples of Ca^{2+} responses of GAD65-expressing interneurons to a male urine exposure under anesthetized conditions. E4. Pseudo-coloured heatmap showing Ca^{2+} responses in the GAD65-expressing interneurons evoked by airflow (0.4LPM) for 2 seconds (red lines) in female mouse AOB. E5. Average Ca^{2+} responses measured in GAD65-expressing interneurons towards opposite sex urine and airflow stimuli (Pink: Male urine, Green: Airflow, Kolmogorov-Smirnov test, Kolmogorov-Smirnov D = 0.73, p-value <0.0001, n = 6). The two red lines show the duration of stimulus.

Modulation of ionotropic glutamate receptor function in the inhibitory interneurons did not cause any anxiety- and depressive-like behaviors

Having observed the activation of GAD65-expressing interneurons towards opposite sex urinary volatiles, we aimed to modulate the function of these interneurons to study their role in pheromone location learning. We targeted the modulation of ionotropic glutamate receptor (iGluR) function using Cre-Lox system. The GluA2 subunit of AMPA receptors, and NR1 subunit of NMDA receptors were deleted in separate cohorts of mice (Figure 2 A,B). These modifications were shown to modulate the synaptic inhibition, and olfactory discrimination abilities in a bidirectional manner (Abraham et al., 2010). We confirmed the deletion of these subunits (heterozygous) by performing PCR and Agarose gel electrophoresis (Figure 2 A2,B2). The decrease in NR1 and GluA2 protein levels in the OB was confirmed by western blotting. We observed ~20-30% decrease in the protein levels compared to control animals (Figure 2A3, B3 NR1: Unpaired one-tailed t-test, p = 0.0313, GluA2: Unpaired one-tailed t-test, p = 0.0347, n = 6).

Although GAD65-expressing interneurons are most abundant in the OB, and are sparsely present in other brain regions, the genetic perturbations are not spatially restricted. Therefore, it can cause some adverse effects. To control this, we carried out a battery of tests evaluating the anxiety- and depressive-like behaviors (Mahajan et al., 2023). On conducting, elevated plus-maze test, we did not observe any changes in the KOs animals' frequency to enter the open arms or the time spent in the open arms compared to control group (Figure 2C: Ordinary one-way ANOVA, Bonferroni's multiple comparison tests p > 0.05). Further, open field test displayed similar time spent in the centre and corner zones by all animals (Figure 2D: Ordinary one-way ANOVA, Bonferroni's multiple comparison tests p > 0.05). These observations confirm that the genetic perturbation did not cause any anxiety-related behaviors in $NR1^{GAD65(+/-)}$ and $GluA2^{GAD65(+/-)}$ animals.

To access the depressive-like symptoms, we conducted forced swim test and tail suspension test. During the forced swim test, animals across groups showed mobility for a similar amount of time (Figure 2E: Ordinary one-way ANOVA, Bonferroni's multiple comparison tests p > 0.05). In addition, the time spent mobile was quantified during tail suspension test. $NR1^{GAD65(+/-)}$, $GluA2^{GAD65(+/-)}$ animals and control mice showed similar duration of mobility (Figure 2F: Ordinary one-way ANOVA, Bonferroni's multiple comparison tests p > 0.05). This indicates the absence of any depressive-like behaviours in these modified animals, and the reliability of behavioral readouts we obtained for the pheromone location learning.

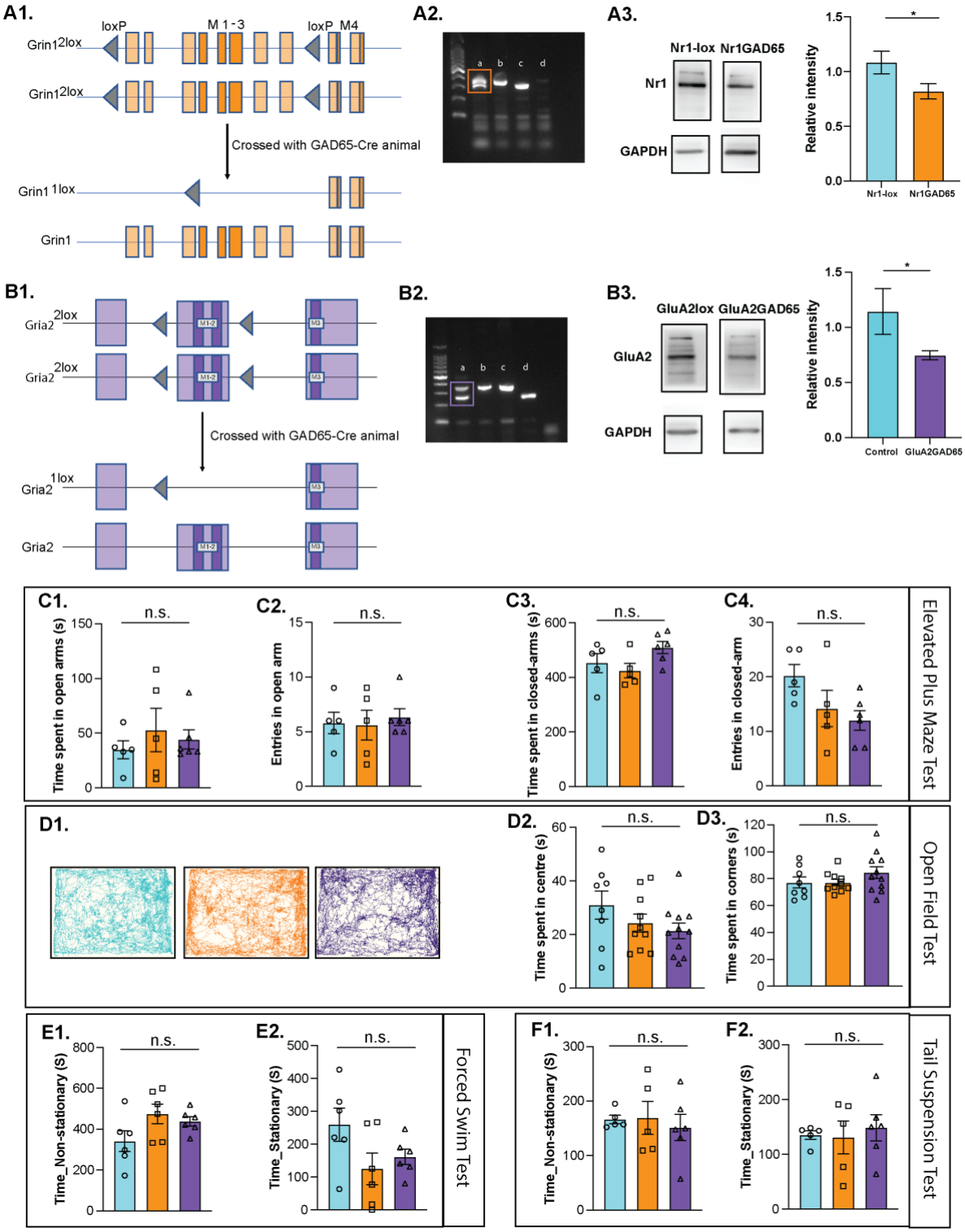

Figure 2: Modulation of NMDA and AMPA receptor function in the inhibitory interneurons did not cause any anxiety- and depressive-like behaviors

A, B: Generation of Knockouts using Cre-Lox system

A1. Scheme of genetic cross used to generate $NR1^{GAD65(+/-)}$ animals.

A2. Agarose gel electrophoresis image of DNA samples taken from a: Heterozygous $NR1^{GAD65(+/-)}$ animal (369 bp and 315 bp), b: NR1-2Lox (369 bp), c: wild-type (315 bp) and d: Blank.

A3. Immunoblots showing expression of NR1 in the olfactory bulb of control and $NR1^{GAD65(+/-)}$ mice. GAPDH was used as a loading control. NR1 expression was reduced in $NR1^{GAD65(+/-)}$ animals.

(Control: 1.083 ± 0.1049, NR1$^{GAD65(+/-)}$: 0.8197 ± 0.0688 mean ± SEM, Unpaired one-tailed t-test, p = 0.0313, n = 6).

B1. Scheme of genetic cross used to generate GluA2$^{GAD65(+/-)}$ animals.

B2. Agarose gel electrophoresis image of DNA samples taken from a: Heterozygous GluA2$^{GAD65(+/-)}$ KO animal (348 bp and 254 bp), b: GluA2-2Lox (348 bp), c: wild-type (254 bp) and d: Blank.

B3. Immunoblots showing expression of GluA2 in the olfactory bulb of control and GluA2$^{GAD65(+/-)}$ mice. GAPDH was used as a loading control. GluA2 expression was reduced in GluA2$^{GAD65(+/-)}$ animals (control: 1.027 ± 0.2051, GluA2: 0.745 ± 0.0400, mean ± SEM Unpaired one-tailed t-test, p = 0.0347, n = 6).

Elevated Plus Maze Test (EPMT):

C1. Time spent in the open arms by different groups of mice were similar (p = 0.6437, F = 0.4558, ordinary one-way ANOVA, Bonferroni's multiple comparison tests, control vs. NR1$^{GAD65(+/-)}$, control vs. GluA2$^{GAD65(+/-)}$, and NR1$^{GAD65(+/-)}$ vs. GluA2$^{GAD65(+/-)}$: p > 0.9999, control and NR1$^{GAD65(+/-)}$ n = 5, GluA2$^{GAD65(+/-)}$ n = 6) (Control shown in cyan, NR1$^{GAD65(+/-)}$ shown in orange and GluA2$^{GAD65(+/-)}$ shown in purple).

C2. Time spent in the closed arms by different groups of mice were similar (p = 0.1158, F = 2.556, ordinary one-way ANOVA, Bonferroni's multiple comparison tests, control vs. NR1$^{GAD65(+/-)}$: p > 0.9999, control vs. GluA2$^{GAD65(+/-)}$ p = 0.4935, NR1$^{GAD65(+/-)}$ vs. GluA2$^{GAD65(+/-)}$: p = 0.1402).

C3. Number of entries in open arms across groups were similar (p = 0.8688, F = 0.1422, ordinary one-way ANOVA, Bonferroni's multiple comparison tests, control vs. NR1$^{GAD65(+/-)}$, control vs. GluA2$^{GAD65(+/-)}$ and NR1$^{GAD65(+/-)}$ vs. GluA2$^{GAD65(+/-)}$: p > 0.9999).

C4. Number of entries in close arms across groups were similar (p = 0.0786, F = 3.113, ordinary one-way ANOVA, Bonferroni's multiple comparison tests, control vs. NR1$^{GAD65(+/-)}$: p = 0.3324, control vs. GluA2$^{GAD65(+/-)}$ p = 0.0889, NR1$^{GAD65(+/-)}$ vs. GluA2$^{GAD65(+/-)}$: p > 0.9999).

Open Field Test (OFT):

D1. Examples of actual tracks taken by the animal, and analyzed using the "Nose-point" feature of EthoVision software.

D2. Time spent at the centre was similar across groups (p = 0.2159, F = 1.627 ordinary one-way ANOVA, Bonferroni's multiple comparison tests, control vs. NR1$^{GAD65(+/-)}$: p = 0.7031, NR1$^{GAD65(+/-)}$ vs. GluA2$^{GAD65(+/-)}$: p>0.9999 control vs. GluA2$^{GAD65(+/-)}$ p = 0.2569, control n = 8, NR1$^{GAD65(+/-)}$ n = 10, GluA2$^{GAD65(+/-)}$ n = 6).

D3. Time spent at the corners were similar across groups (p = 0.2853, F = 1.317 Ordinary one-way ANOVA, Bonferroni's multiple comparison test, control vs. NR1$^{GAD65(+/-)}$: p >0.9999, NR1$^{GAD65(+/-)}$ vs. GluA2$^{GAD65(+/-)}$: p = 0.5046, control vs. GluA2$^{GAD65(+/-)}$ p = 0.5745).

Forced Swim Test (FST):

E1. There were no significant differences in the time spent mobile across groups (p = 0.1006, F = 2.687, ordinary one-way ANOVA, Bonferroni's multiple comparison tests, control vs. NR1$^{GAD65(+/-)}$: p = 0.1219, control vs. GluA2$^{GAD65(+/-)}$ p = 0.3684, NR1$^{GAD65(+/-)}$ vs. GluA2$^{GAD65(+/-)}$: p > 0.9999, control and NR1$^{GAD65(+/-)}$ n = 5, GluA2$^{GAD65(+/-)}$ n = 6).

E2. There were no significant differences in the time spent immobile across groups (p = 0.1006, F = 2.687, ordinary one-way ANOVA, Bonferroni's multiple comparison tests, control vs. NR1$^{GAD65(+/-)}$: p = 0.1219, control vs. GluA2$^{GAD65(+/-)}$ p = 0.3684, NR1$^{GAD65(+/-)}$ vs. GluA2$^{GAD65(+/-)}$: p > 0.9999).

Tail Suspension Test (TST):

F1. There were no significant differences in the time spent mobile across groups (p = 0.8402, F = 0.1765, ordinary one-way ANOVA, Bonferroni's multiple comparison tests, control vs. NR1$^{GAD65(+/-)}$, control vs. GluA2$^{GAD65(+/-)}$, and NR1$^{GAD65(+/-)}$ vs. GluA2$^{GAD65(+/-)}$: p > 0.9999, control and NR1$^{GAD65(+/-)}$ n = 5, GluA2$^{GAD65(+/-)}$ n = 6).

F2. There were no significant differences in the time spent immobile across groups (p = 0.8474, F = 0.1677, ordinary one-way ANOVA, Bonferroni's multiple comparison tests, control vs. NR1$^{GAD65(+/-)}$, control vs. GluA2$^{GAD65(+/-)}$, and NR1$^{GAD65(+/-)}$ vs. GluA2$^{GAD65(+/-)}$: p > 0.9999).

Controls are shown in cyan, NR1$^{GAD65(+/-)}$ animals are shown in orange, and GluA2$^{GAD65(+/-)}$ animals

are shown in purple. Data are shown in mean ± SEM.

Ionotropic glutamate receptor functions of GAD65-expressing inhibitory interneurons are necessary for pheromone location learning and memory

Upon confirming no other behavioral disorders due to the genetic perturbations, we performed pheromone detection assay in $NR1^{GAD65(+/-)}$ and $GluA2^{GAD65(+/-)}$ female mice. Animals were allowed to explore an arena, where 100 µl of male urine along with soiled bedding from opposite sex was kept in a petri dish at the centre of arena. We observed similar time spent near the pheromone-containing chamber across different groups of mice (Figure 3A:Ordinary one-way ANOVA, Bonferroni's multiple comparison tests, $p > 0.9999$, $n = 8$). Next, we subjected the animals to pheromone place preference assay. To investigate the animals' preference towards any chamber, testing phase (TP) was conducted as explained (see materials and methods). The preference was quantified based on the time spent and active attempts done towards the respective zone. Animals across groups did not display specific preference towards any chambers on the last day of TP (Figure 3B: Ordinary Two-way ANOVA, Day 4 $p > 0.05$).

Next, we trained the animals to associate the volatiles and non-volatiles with the specific hole-size of the plates, during a 15-day long training phase (TrP). Animals showed consistent attempts to sample the pheromones, quantified by the time spent and active attempts, throughout the TrP, i.e. on training day 1 (TrD1), 7 and 15 (supplementary figure S1). 15 days after the TrP was over, we quantified the memory of pheromone location, on memory testing day 15 (MD 15). For testing the memory, we used a new but similar setup to avoid the presence of any pheromonal cues while probing the memory of pheromone locations. We observed an increased preference towards pheromone zone by control females, shown by significantly higher time spent and greater number of active attempts (C1-C3: Examples of tracks taken by the animals on memory testing day. Figure 3D1, E1: Paired two-tailed student's t-test, $p < 0.05$, $n = 15$). However, $GluA2^{GAD65(+/-)}$ females showed similar time spent and number of active attempts towards pheromonal and neutral stimulus chambers (Figure 3D2, E2, Paired two-tailed student's t-test, $p > 0.05$). Similar results were obtained with $NR1^{GAD65(+/-)}$ females as well (Figure 3D3, E3, Paired two-tailed student's t-test, $p > 0.05$). These results prove the essential role of iGluRs in regulating pheromone location learning and memory. To probe the memory of pheromone chamber on early time point, we conducted pheromone place preference assay with another set of female mice and checked their memory 7 days post-TrP. We observed lack of memory on MD7 shown by similar time spent and active attempts towards both the chambers (Supplementary Figure S2). Previous studies report the modulation of sniffing during odor discrimination as well as social communication in animals (Uchida et al., 2006; Wachowiak, 2011; Wesson, 2013; Abraham et al., 2014; Bhattacharjee et al., 2019). To study if the iGluR modifications cause any differences in the sniffing we quantified their sniffing toward opposite sex urine volatiles under head-restrained conditions (Abraham et al., 2012; Bhattacharjee et al., 2019; Pardasani et al., 2021; Mahajan et al., 2024). We did not observe any changes in sniffing frequency across different experimental groups of mice, indicating that the pheromone location learning and memory deficits we report here is not due to the differences in their sampling behaviors (Supplementary Figure S3).

Expression of Arc, an immediate early gene, during memory recall indicates neural activity. Previously we have seen differential expression of Arc in the OB, somatosensory cortex (SSC) and Dentate Gyrus (DG) of animals displaying lack of pheromone location memory (Pardasani et al., 2021). To understand the neuronal activation pattern during MD15 across groups, we performed immunohistochemistry against Arc antibody. When quantified, we observed significantly less number of Arc+ cells in MOB, AOB, SSC and DG (Figure 3 F1 – F8: Ordinary one-way ANOVA, Bonferroni's multiple comparisons test, $p < 0.05$, $n = 3$). This decrease in the Arc+ cells in $NR1^{GAD65(+/-)}$ and $GluA2^{GAD65(+/-)}$ females on MD15 explains the impaired learning and memory of pheromone locations shown by these mice.

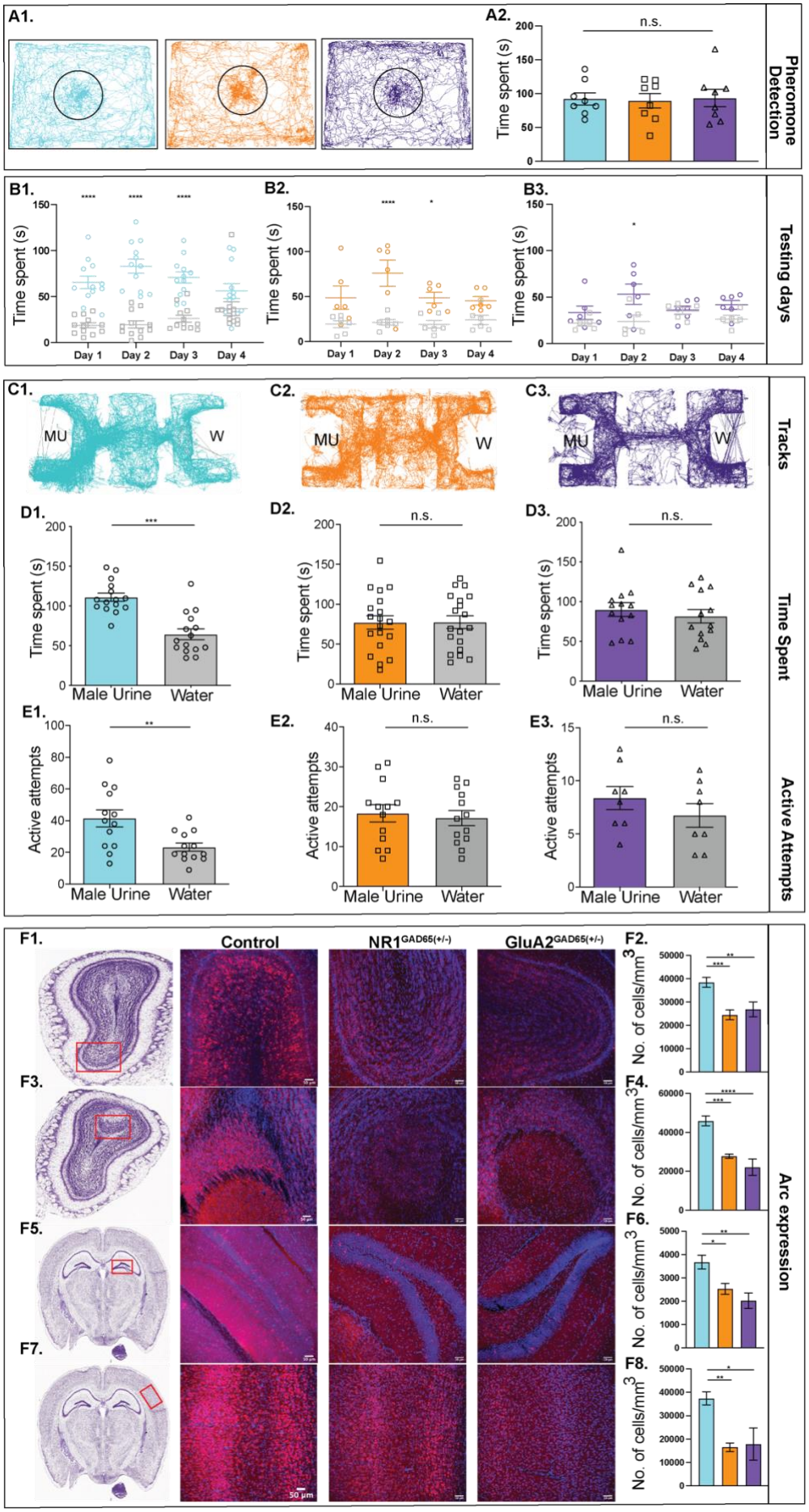
A1.
A2.
n.s.
Time spent (s)
Pheromone Detection
B1.
B2.
B3.
Time spent (s)
Day 1
Day 2
Day 3
Day 4
Testing days
C1.
C2.
C3.
MU
W
Tracks
D1.
D2.
D3.
Time spent (s)
Male Urine
Water
Time Spent
E1.
E2.
E3.
Active attempts
Active Attempts
F1.
F2.
F3.
F4.
F5.
F6.
F7.
F8.
Control
NR1GAD65(+/-)
GluA2GAD65(+/-)
No. of cells/mm3
Arc expression
50 µm

Figure 3: Learning and memorizing pheromone locations require functional NMDARs and AMAPARs in GAD65-expressing interneurons.

A1,A2. Pheromonal detection readout measured by the time spent by mice to explore pheromone-containing petri dish in an open arena. A1. Tracks taken by the animal while exploring the pheromone-containing petri dish in an open arena and were analyzed using the "Nose-point" feature of EthoVision software. A2. Time spent by different groups of mice was similar ($p = 0.9626$, $F = 0.03817$ Ordinary one-way ANOVA, Bonferroni's multiple comparison tests, control vs. $NR1^{GAD65(+/-)}$, control vs. $GluA2^{GAD65(+/-)}$, and $NR1^{GAD65(+/-)}$ vs. $GluA2^{GAD65(+/-)}$: $p > 0.9999$, $n = 8$).

B1,B2,B3. Time spent near the male urine chamber (cyan) and water chamber (grey) by control female mice during the testing phase (Ordinary Two-way ANOVA, followed by Bonferroni's multiple comparison test, Day 1 $p = <0.0001$, Day 2 $P = <0.0001$, Day 3 $p = <0.0001$, Day 4 $p = 0.1243$). Time spent near the male urine chamber (orange) and water chamber (grey) by $NR1^{GAD65(+/-)}$ females. (Ordinary Two-way ANOVA, Day 1 $p = 0.0503$, Day 2 $P < 0.0001$, Day 3 $p = 0.0488$, Day 4 $p = 0.2672$). Time spent near the male urine chamber (purple) and water chamber (grey) by $GluA2^{GAD65(+/-)}$ females. (Ordinary Two-way ANOVA, Day 1 $p = 0.9123$, Day 2 $P = 0.0110$, Day 3 $p > 0.999$, Day 4 $p = 0.4264$).

C1,C2,C3. Tracks obtained by the nose-point feature of EthoVision software (8.5 XT) during the memory day. MU represents the male urine chamber, and W represents the water chamber.

D1. Significantly longer time was spent near the male urine chamber by control females on memory testing day, MD 15 ($p = 0.0001$, paired two-tailed student's t-test, $n = 15$).

D2. $NR1^{GAD65(+/-)}$ females showed similar time spent near both the chambers on MD 15 ($p = 0.9492$, paired two-tailed student's t-test, $n = 19$).

D3. $GluA2^{GAD65(+/-)}$ females displayed similar time spent near both the chambers on MD 15 ($p = 0.5516$, paired two-tailed student's t-test, $n = 13$).

E1. Control females exhibited a greater number of active attempts to the male urine chamber on memory testing day, MD 15 ($p = 0.0003$, paired two-tailed student's t-test, $n = 13$).

E2. $NR1^{GAD65(+/-)}$ females displayed similar number of active attempts to both chambers on memory testing day, MD 15 ($p = 0.6574$, paired two-tailed student's t-test, $n = 13$).

E3. $GluA2^{GAD65(+/-)}$ females showed a similar number of active attempts to both chambers on memory testing day, MD 15 ($p = 0.0819$, paired two-tailed student's t-test, $n = 8$).

F1. Immunofluorescence images of MOB on MD15 of control, $NR1^{GAD65(+/-)}$ and $GluA2^{GAD65(+/-)}$. (Blue: DAPI, Red: Arc, Scale bar: 50 µm).

F2. Significantly lower number of Arc positive cells were observed in the MOB of $NR1^{GAD65(+/-)}$ and $GluA2^{GAD65(+/-)}$ animals compared to control mice ($p < 0.0001$, $F = 18.36$, Ordinary one-way ANOVA, Bonferroni's multiple comparisons test, Control vs $NR1^{GAD65(+/-)}$: $p < 0.0001$, $NR1^{GAD65(+/-)}$ vs $GluA2^{GAD65(+/-)}$: $p > 0.9999$, Control vs $GluA2^{GAD65(+/-)}$: $p = 0.0002$, $n = 3$).

F3. Immunofluorescence images of AOB on MD15 of control, $NR1^{GAD65(+/-)}$ and $GluA2^{GAD65(+/-)}$.

F4. Significantly lower number of Arc positive cells were observed in the AOB of $NR1^{GAD65(+/-)}$ and $GluA2^{GAD65(+/-)}$ heterozygous knockout animals compared to control mice ($p < 0.0001$, $F = 16.52$, Ordinary one-way ANOVA, Bonferroni's multiple comparisons test, Control vs $NR1^{GAD65(+/-)}$: $p = 0.0007$, $NR1^{GAD65(+/-)}$ vs $GluA2^{GAD65(+/-)}$: $p = 0.5658$, Control vs $GluA2^{GAD65(+/-)}$: $p < 0.0001$, $n = 3$).

F5. Immunofluorescence images of hippocampus on MD15 of control, $NR1^{GAD65(+/-)}$ and $GluA2^{GAD65(+/-)}$.

F6. Significantly lower number of Arc positive cells were observed in the Dentate Gyrus of $NR1^{GAD65(+/-)}$ and $GluA2^{GAD65(+/-)}$ heterozygous knockout animals compared to control mice ($p = 0.0016$, $F = 8.376$, Ordinary one-way ANOVA, Bonferroni's multiple comparisons test, Control vs $NR1^{GAD65(+/-)}$: $p = 0.0352$, $NR1^{GAD65(+/-)}$ vs $GluA2^{GAD65(+/-)}$: $p = 0.6882$, Control vs $GluA2^{GAD65(+/-)}$: $p = 0.0014$, $n = 3$).

F7. Immunofluorescence images of SSC on MD15 of control, $NR1^{GAD65(+/-)}$ and $GluA2^{GAD65(+/-)}$.

F8. Significantly lower number of Arc positive cells were observed in the SSC of $NR1^{GAD65(+/-)}$ and $GluA2^{GAD65(+/-)}$ heterozygous knockout animals compared to control mice ($p = 0.0027$, $F = 7.562$, Ordinary one-way ANOVA, Bonferroni's multiple comparisons test, Control vs $NR1^{GAD65(+/-)}$: $p = 0.0061$, $NR1^{GAD65(+/-)}$ vs $GluA2^{GAD65(+/-)}$: $p > 0.9999$, Control vs $GluA2^{GAD65(+/-)}$: $p = 0.0105$, $n = 3$).

Ionotropic glutamate receptor functions in the inhibitory interneurons of accessory olfactory bulb regulates pheromone location learning and memory

Having observed the pheromone location learning and memory deficits in GAD65-expressing interneuron-specific iGluR heterozygous knockouts, we decided to probe the role of inhibitory interneuron network of OB in regulating pheromone location learning and memory. Earlier we have shown that modulating the inhibitory network can affect olfactory discrimination abilities (Abraham et al., 2010; Gschwend et al., 2015; Pardasani et al., 2023). To modulate the inhibitory network of MOB, we injected AAV5-Cre expressing viral particles in the granule cell layer (GCL) of OB in NR1Lox and GluA2Lox female mice, using a well-established stereotaxic coordinates (Abraham et al., 2010; Gschwend et al., 2015). As we have observed the involvement of AOB neurons in pheromone location learning, we also targeted AOB interneurons using stereotaxic approaches. In three different groups of mice – control, NR1Lox and GluA2Lox, the iGluR functions were modulated in the inhibitory network of MOB and AOB. These modified mice are referred as $NR1^{\Delta OB}$, $GluA2^{\Delta AOB}$ henceforth. The behavioral training was started 2-3 weeks after the surgery. Pheromone detection abilities of these animals were unhampered (Figure 4B, Ordinary one-way ANOVA, Bonferroni's multiple comparison tests, $p > 0.05$). After 15 days of pheromone location learning training, we evaluated their memory on post-training day 15. While we observed enhanced time spent and number of active attempts towards pheromone chamber by the control female mice (Figure 4C1-E1, Paired two-tailed student's t-test, $p < 0.05$), similar time spent, and number of active attempts were made by $NR1^{\Delta OB}$, $GluA2^{\Delta OB}$ females (Figures 4C2-E2, C3-E3, Paired two-tailed student's t-test, $p > 0.05$). These results confirm the role of ionotropic glutamate receptors of the OB in regulating the learning and memory of pheromone locations.

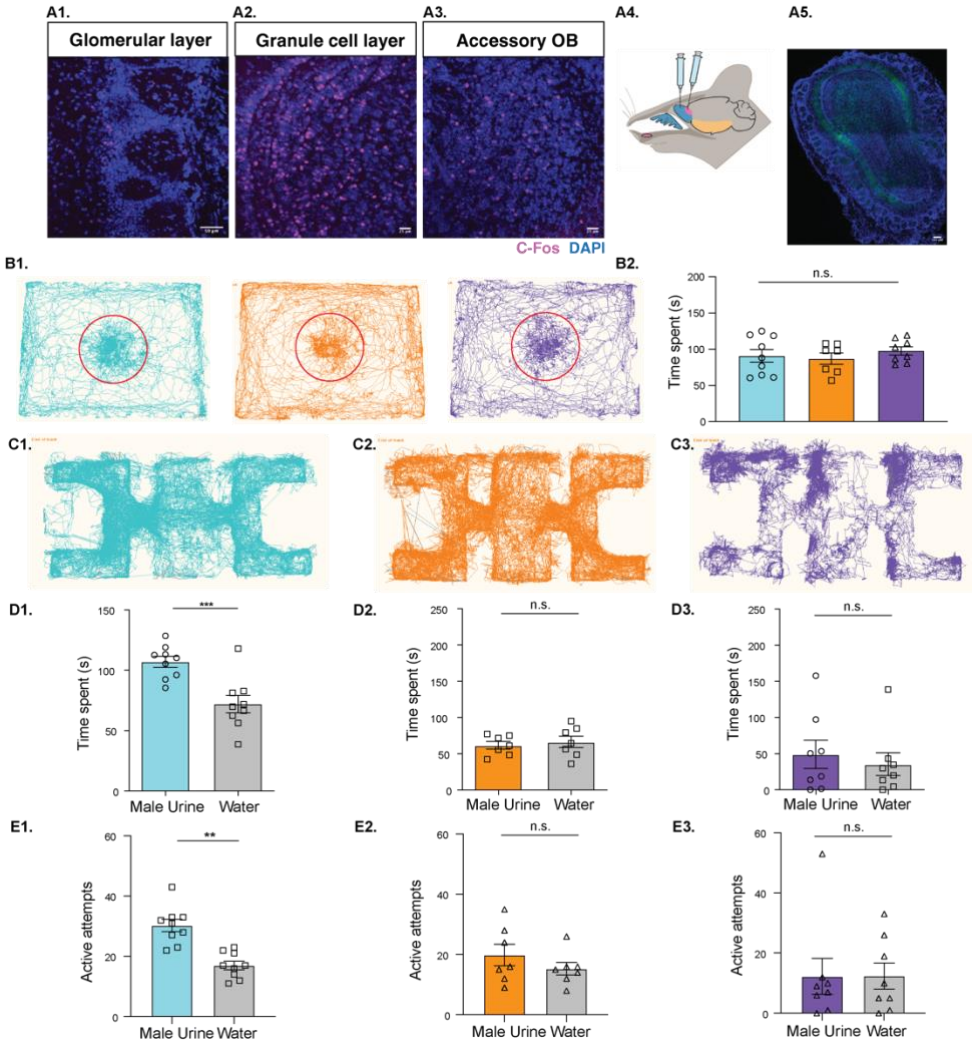

Figure 4: Modification of ionotropic glutamate receptors in the inhibitory interneurons of olfactory bulb results in the deficits of pheromone location learning

A1,A2,A3. Immunofluorescence images showing c-Fos expression in different regions of the main OB (glomerular layer and granule cell layer) and accessory OB, upon male urine exposure (Blue: DAPI, Magenta: c-Fos, scale bar = 25 µm).

A4. Diagrammatic representation of stereotaxic delivery of AAV particles in the olfactory bulb.

A5. GCL interneurons expressing EGFP after AAV-mediated Cre delivery.

B1. Examples of tracks taken by the animal and analyzed using the "Nose-point" feature of EthoVision software in a pheromone detection assay. As seen by the tracks, different experimental groups spent similar time near petri-dish containing male urine and soiled bedding shown in a red circle.

B2. Similar time was spent by different experimental groups of female mice in a pheromone detection assay (Ordinary one-way ANOVA, $p = 0.6247$, $F = 0.4811$, Bonferroni's multiple comparison tests, control vs. $NR1^{\Delta OB}$, control vs. $GluA2^{\Delta OB}$, and $NR1^{\Delta OB}$ vs. $GluA2^{\Delta OB}$: $p > 0.9999$). Data are shown in mean ± SEM. (Control n = 9, $NR1^{\Delta OB}$ n = 7, $GluA2^{\Delta OB}$ n = 8).

C1,C2,C3. Examples of tracks taken by different experimental groups on memory testing day in pheromone place preference assay.

D1. Control female mice spent significantly more time near the male urine chamber on a memory testing day, MD 15, indicating accurate pheromone location learning and memory (paired two-tailed student's t-test, $p = 0.0001$, n = 9).

D2. $NR1^{\Delta OB}$ females exhibited memory impairment, as they spent a similar amount of time near both chambers on memory testing day, MD 15 (paired two-tailed student's t-test, $p = 0.4677$, n = 7).

D3. $GluA2^{\Delta OB}$ females displayed a lack of memory by spending similar time near both chambers on memory testing day, MD 15 (paired two-tailed student's t-test, $p = 0.9689$, n = 8).

E1. Higher number of active attempts were made by control female mice on memory testing day, MD 15 ($p = 0.0039$, paired two-tailed student's t-test, n = 9).

E2. $NR1^{\Delta OB}$ females performed a similar number of active attempts towards both chambers on memory testing day, MD 15, indicating impaired pheromone location learning and memory (paired two-tailed student's t-test, $p = 0.5625$, n = 7).

E3. $GluA2^{\Delta OB}$ females performed a comparable number of active attempts towards both chambers on memory testing day, MD 15, indicating compromised pheromone location learning and memory (paired two-tailed student's t-test, $p > 0.9999$, n = 8).

Mouse AOB plays a critical role in pheromone information processing. To further investigate even perturbing the AOB inhibitory network alters the pheromone location learning abilities, we kept the MOB iGluRs intact, and modified the AOB circuits. We injected AAV5-Cre viral particles in the AOB of NR1Lox and GluA2Lox female animals. They are referred to as $NR1^{\Delta AOB}$ and $GluA2^{\Delta AOB}$ henceforth. After three weeks of surgery, their pheromone detection abilities were assessed and compared with that of control mice. $NR1^{\Delta AOB}$ and $GluA2^{\Delta AOB}$ female mice showed undisturbed pheromone detection abilities as observed by the time spent near a male urine-containing petri dish (Figure 5B, Ordinary one-way ANOVA, Bonferroni's multiple comparison tests, $p > 0.05$). Mice were then trained to associate specific hole sizes with pheromone containing chamber and neutral stimulus chamber for 15 days. After 15 days their memory was evaluated. Control mice showed enhanced time spent and number of active attempts towards pheromone chamber compared to neutral stimulus chamber (Figure 5C1-E1, Paired two-tailed student's t-test, $p < 0.05$). However, similar time spent, and number of active attempts were made by $NR1^{\Delta AOB}$, $GluA2^{\Delta AOB}$ females (Figures 5C2-E2, C3-E3, Paired two-tailed student's t-test, $p > 0.05$). These results confirm the role of ionotropic glutamate receptors of the AOB in regulating the learning and memory of pheromone locations. Our results thus prove the important role of iGluRs on GAD65 expressing interneurons both in MOB and AOB, and thereby the synaptic inhibitory network in regulating the pheromone location learning and memory.

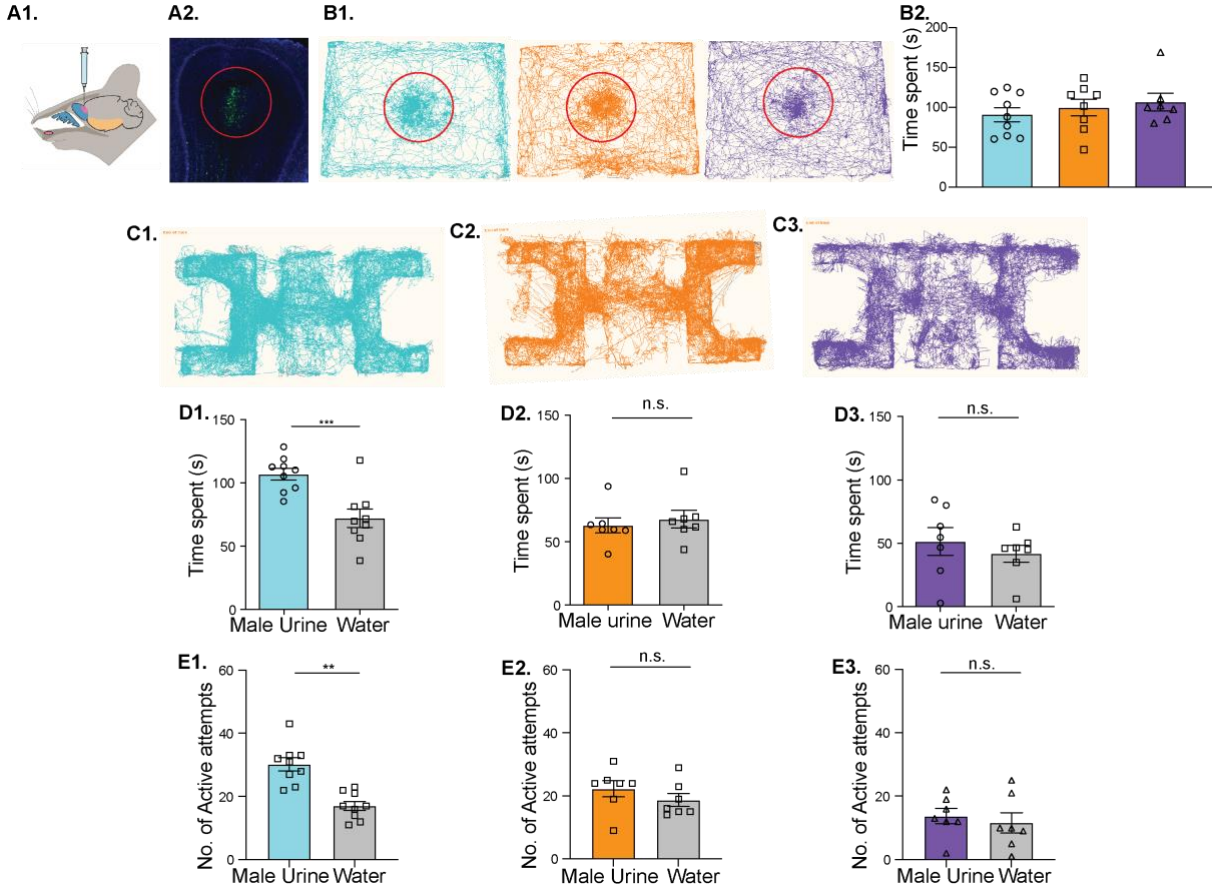

Figure 5: Ionotropic glutamate receptor functions in the accessory olfactory bulb neuronal circuitry regulate pheromone location learning

A1. Diagrammatic representation of stereotaxic delivery of AAV particles in the accessory olfactory bulb.

A2. Expression of EGFP as an indication of AAV-mediated Cre expression in AOB.

B1. Examples of tracks taken by the animal and analyzed using the "Nose-point" feature of EthoVision software in a pheromone detection assay. As seen by the tracks, different experimental groups spent similar time near petri-dish containing male urine and soiled bedding shown in a red circle.

B2. Similar time was spent by different experimental groups of female mice in a pheromone detection assay (Ordinary one-way ANOVA, $p = 0.6139$, $F = 0.5507$ Bonferroni's multiple comparison tests, control vs. $NR1^{\Delta AOB}$: $p > 0.05$, control vs. $GluA2^{\Delta AOB}$ $p = 0.8574$, $NR1^{\Delta AOB}$ vs. $GluA2^{\Delta AOB}$: $p > 0.05$). Data are mean ± SEM. (Control n = 9, $NR1^{\Delta AOB}$ n = 8, $GluA2^{\Delta AOB}$ n = 7).

C1,C2,C3. Examples of tracks taken by different experimental groups on memory testing day in pheromone place preference assay.

D1. Control female mice spent significantly more time near the male urine chamber on a memory testing day, MD 15, indicating accurate pheromone location learning and memory (paired two-tailed student's t-test, $p = 0.0001$, n = 9).

D2. $NR1^{\Delta AOB}$ females exhibited memory impairment, as they spent a similar amount of time near both chambers on memory testing day, MD 15 (Paired two-tailed student's t-test, $p = 0.5734$, n = 7).

D3. $GluA2^{\Delta AOB}$ females displayed a lack of memory by spending similar time near both chambers on memory testing day, MD 15 (Paired two-tailed student's t-test, $p = 0.2159$, n = 7).

E1. Higher number of active attempts were made by control female mice on memory testing day, MD 15 (Paired two-tailed student's t-test, $p = 0.0039$, n = 9).

E2. NR1$^{\Delta AOB}$ females performed a similar number of active attempts towards both chambers on memory testing day, MD 15, indicating impaired pheromone location learning and memory (Paired two-tailed student's t-test p = 0.3906, n = 7).
E3. GluA2$^{\Delta AOB}$ females performed a comparable number of active attempts towards both chambers on memory testing day, MD 15, indicating compromised pheromone location learning and memory (Paired two-tailed student's t-test, p = 0.4062, n = 8).

Discussion

Rodents' olfactory system plays a major role in socio-sexual communication (Dulac and Kimchi, 2007; Chen and Hong, 2018). Urinary scent marks, comprised of volatile and non-volatile pheromones, have been commonly used by mice for such communication (Arakawa et al., 2008; Demir et al., 2020). The volatile components of urine can reflect the reproductive potential of a male mouse as their production is testosterone-dependent (Schwende et al., 1986). Therefore, the reproductive success of a female mouse would be controlled by their ability to remember the pheromone locations in wild. As the pheromones are streaked on objects of different sizes and shapes, the involvement of somatosensory system is expected in this process. We made use of these observations to design our behavioral paradigm for studying the neural mechanisms of pheromone location learning and memory (Pardasani et al., 2021; Jabarin et al., 2022). Further our study took the advantage of spatio-temporal specific deletion of iGluRs from the inhibitory network of MOB and AOB by using Cre-Lox system and viral vector mediated gene delivery (Abraham et al., 2010).

Both main and accessory olfactory bulbs are involved in pheromonal information processing (Ma, 2010; Mucignat-Caretta et al., 2012). The behavioral assay we used in this study has been shown to be an ideal paradigm to investigate the engagement of olfactory and whisker systems in pheromone location learning and memory (Pardasani et al., 2021). Therefore, we decided to modify the MOB and AOB circuits, and probe animals' ability to learn and memorize pheromone location using this paradigm. On training mice in this pheromonal place preference assay, we observed many c-Fos positive cells, a neuronal activity marker, among the interneurons of both MOB and AOB circuits. To confirm the activation of inhibitory network, we expressed GCaMP6f driven by GAD-65, which is expressed by majority of the inhibitory interneurons of MOB and AOB (Burton, 2017; Maksimova et al., 2019). AOB interneurons showed higher calcium activity in response to urinary volatiles compared to airflow stimuli (Figure 1). To modulate the inhibitory actions, we targeted iGluRs of GAD65 expressing interneurons and their deletion did not result in any anxiety- and depressive-like symptoms (Figure 2). While the heterozygous knockouts of GluA2 (subunit of AMPARs) and NR1 (subunit of NMDARs) showed intact pheromone detection abilities, pheromone location memory was reduced compared to control mice. Correlated reduction in the number of Arc expressing cells were observed in the knockout mice (Figure 3). Further to make the perturbation specific to olfactory areas, interneurons of both MOB & AOB, and AOB alone were targeted by making use of Cre-Lox system and stereotaxic delivery of viral vectors. In both these cases pheromone location memory was compromised compared to control animals. This reveals the central role of iGluRs in MOB and AOB inhibitory network in regulating pheromone location learning and memory (Figures 4 and 5).

To study the neuronal mechanisms, it is critical to form ethologically relevant associations in a learning paradigm. The urinary scent marks communicates the competitive ability and identity of individual male mouse (Hurst and Beynon, 2004; Brennan and Kendrick, 2006). Therefore, to mimic the natural conditions, we designed the experimental paradigm, where the animals have to use both olfactory and whisker systems during learning. The whisker system can potentially be involved while sniffing the pheromones streaked on different objects. Earlier studies report coordinated action of sniffing and whisking, which is regulated by respiratory centers in the ventral medulla (Welker, 1964; Moore et al., 2013; Ranade et al., 2013). This kind of multimodal sampling might be happening during the

exploration of pheromone locations. Earlier experiments done by Garcia proved the relevance of association when two stimuli are combined. The association of tasty water with a noxious drug worked better compared to a bright-noisy water-noxious stimulus association in avoiding a gustatory stimulus (Garcia and Koelling, 1966). Our training, where animals had to learn to associate certain hole size with pheromonal cues, worked well and mice exhibited a robust memory of this association (Figure 1).

Odorants evoke spatiotemporal specific glomerular activity patterns in the olfactory bulb, which is the first relay station in olfactory information processing (Mori et al., 1999; Abraham et al., 2004; Schaefer and Margrie, 2007; Abraham et al., 2014; Bhattacharjee et al., 2019). The overlapping patterns of activity evoked by complex odorants are refined and decorrelated by the inhibitory network of OB before odor information is sent to higher centres (Abraham et al., 2010; Gschwend et al., 2015). We observed many activated cells among the inhibitory network of MOB and AOB in response to urinary volatiles (Figure 1). Therefore we modulated the synaptic inhibition by targeting iGluRs on GAD65 expressing interneurons (Figure2). While removing the GluA2 subunit of AMPARs increase the inflow of calcium, deleting the essential subunit of NMDARs would result in non-functional NMDARs, which may cause decrease of Ca^{2+} levels. These modifications trigger bidirectional shift of inhibition in the OB network (Abraham et al., 2010). Whenever the optimal inhibition is varied in the OB circuits, it resulted in the alterations of odor discrimination abilities in mice (Gschwend et al., 2015; Mahajan et al., 2024). Vomeronasal and main olfactory systems are more integrated in processing the information from volatile and non-volatile urinary pheromones (Liberles and Buck, 2006; Spehr et al., 2006; Leinders-Zufall et al., 2007; Ma, 2012). Therefore, to study the neural mechanisms we undertook a genetic approach to modify iGluRs present on the GAD65-expressing interneurons of both MOB and AOB and probed their pheromone location memory after training. iGluR-modified mice did not show the memory of pheromone locations compared to control animals (Figure 3). The learning and memory deficit was independent of their intact sampling behaviors (Supplementary Figures S1 & S3).

Deletion of GluA2 or NR1 from inhibitory interneurons would result in a global modulation of inhibitory actions, considering the extensive lateral connectivity in MOB and AOB (Brennan and Keverne, 1997; Urban, 2002; Schoppa and Urban, 2003; Arevian et al., 2008; Hendrickson et al., 2008). Apart from this, there are other sources of glutamatergic inputs on inhibitory neurons, for example on granule cells (Balu et al., 2007). As the synaptic inhibition has been shown to be critical for decorrelating the overlapping patterns of activity in MOB, and the sex-specific cue selectivity of AOB neurons, we decided to make our modulations specific to MOB and AOB circuits by using stereotaxic approaches (Hendrickson et al., 2008; Gschwend et al., 2015). For targeting the MOB interneurons, we used a well-established stereotaxic coordinates, and for the AOB, we optimized the coordinates (Kang et al., 2009; Abraham et al., 2010; Gschwend et al., 2015). Modulation of iGluRs in MOB and AOB inhibitory circuits resulted in pheromone location learning and memory deficits (Figure 4). This can be explained by the reports on the role of iGluRs in long term potentiation and depression, the mechanisms that underly learning and memory (Chung et al., 2003; Watt et al., 2004).

Pheromones can promote associative learning (Brennan, 2010). The non-volatile urinary proteins from males attract naïve females. These proteins not only attract females, but also promote the learning of urinary volatiles (Moncho-Bogani et al., 2005; Ramm et al., 2008). As we kept the bedding with urinary proteins from males in front of the pheromone chamber from where the urinary volatiles emanated, it helped the associative learning, which was reflected in the memory readouts of all control mice used in the study. This was hampered in case of iGluR modification in the AOB inhibitory circuits (Figure 3 and 5). These results confirm the importance of AOB inhibitory circuits in regulating pheromone location learning and memory. The synaptic activation of neurons leads to the expression of immediate early genes, for example, Activity-regulated cytoskeleton-associated (Arc) protein. Newly formed Arc mRNA is accumulated at the strongly activated synapses. The localization of Arc mRNA to active synapses and their transcription requires intact functioning of NMDARs and AMPARs (Steward and

Worley, 2001; Rao et al., 2006). Therefore, iGluR modulations will lead to compromised expression of Arc protein, which was observed in iGluR heterozygous knockouts (Figure 3).

Karlson and Luscher defined pheromones as "airborne chemical signals released by an individual into the environment and affecting the physiology and behavior of other members of the same species" (Karlson and Luscher, 1959). Although humans lack neuronal elements in VNO, activation of hypothalamus has been observed in response to pheromone-like compounds (Trotier et al., 2000; Savic et al., 2001; Witt et al., 2002). Further evidences are present for the perception and behavioral changes caused by pheromones in human subjects. As examples, synchronization of menstrual cycles and the effect on ovulation in roommates, probably mediated by sweat (Stern and McClintock, 1998), sniffing sex-steroid derived compound resulting in mood changes and arousal (Bensafi et al., 2004), social odorants causing modulations in mood (Lundstrom and Olsson, 2005) etc. All these observations confirm chemical communication in humans, leaving the involvement of olfactory system and underlying neural mechanisms as open questions. As olfactory functions are affected under many disease conditions (Doty, 2012; Croy et al., 2014; Doty, 2017; Bhattacharjee et al., 2020; Abraham, 2022), and in long COVID (Pardasani and Abraham, 2022; Bhowmik et al., 2023; Davis et al., 2023; Pandey et al., 2024), investigating the neural mechanisms of chemical communication using appropriate animal models and experimental methods become indispensable (Pardasani et al., 2021; Mahajan et al., 2023).

References

Abraham NM (2022) Olfactory-action meter for precise quantification of olfactory dysfunctions and neurocognitive deficits. US Patent 11786164.

Abraham NM, Guerin D, Bhaukaurally K, Carleton A (2012) Similar odor discrimination behavior in head-restrained and freely moving mice. PLoS One 7:e51789.

Abraham NM, Vincis R, Lagier S, Rodriguez I, Carleton A (2014) Long term functional plasticity of sensory inputs mediated by olfactory learning. Elife 3:e02109.

Abraham NM, Spors H, Carleton A, Margrie TW, Kuner T, Schaefer AT (2004) Maintaining accuracy at the expense of speed: stimulus similarity defines odor discrimination time in mice. Neuron 44:865-876.

Abraham NM, Egger V, Shimshek DR, Renden R, Fukunaga I, Sprengel R, Seeburg PH, Klugmann M, Margrie TW, Schaefer AT, Kuner T (2010) Synaptic Inhibition in the Olfactory Bulb Accelerates Odor Discrimination in Mice. Neuron 65:399-411.

Arakawa H, Blanchard DC, Arakawa K, Dunlap C, Blanchard RJ (2008) Scent marking behavior as an odorant communication in mice. Neurosci Biobehav Rev 32:1236-1248.

Arevian AC, Kapoor V, Urban NN (2008) Activity-dependent gating of lateral inhibition in the mouse olfactory bulb. Nat Neurosci 11:80-87.

Aungst JL, Heyward PM, Puche AC, Karnup SV, Hayar A, Szabo G, Shipley MT (2003) Centre-surround inhibition among olfactory bulb glomeruli. Nature 426:623-629.

Balu R, Pressler RT, Strowbridge BW (2007) Multiple modes of synaptic excitation of olfactory bulb granule cells. J Neurosci 27:5621-5632.

Belluscio L, Koentges G, Axel R, Dulac C (1999) A map of pheromone receptor activation in the mammalian brain. Cell 97:209-220.

Bensafi M, Tsutsui T, Khan R, Levenson RW, Sobel N (2004) Sniffing a human sex-steroid derived compound affects mood and autonomic arousal in a dose-dependent manner. Psychoneuroendocrinology 29:1290-1299.

Bhattacharjee AS, Joshi SV, Naik S, Sangle S, Abraham NM (2020) Quantitative assessment of olfactory dysfunction accurately detects asymptomatic COVID-19 carriers. EClinicalMedicine 28:100575.

Bhattacharjee AS, Konakamchi S, Turaev D, Vincis R, Nunes D, Dingankar AA, Spors H, Carleton A, Kuner T, Abraham NM (2019) Similarity and Strength of Glomerular Odor Representations Define a Neural Metric of Sniff-Invariant Discrimination Time. Cell Rep 28:2966-+.

Bhowmik R, Pardasani M, Mahajan S, Magar R, Joshi SV, Nair GA, Bhattacharjee AS, Abraham NM (2023) Persistent olfactory learning deficits during and post-COVID-19 infection. Curr Res Neurobiol 4:100081.

Brennan PA (2010) Pheromones and Mammalian Behavior. In: The Neurobiology of Olfaction (Menini A, ed). Boca Raton (FL).

Brennan PA, Keverne EB (1997) Neural mechanisms of mammalian olfactory learning. Prog Neurobiol 51:457-481.

Brennan PA, Kendrick KM (2006) Mammalian social odours: attraction and individual recognition. Philos Trans R Soc Lond B Biol Sci 361:2061-2078.

Burton SD (2017) Inhibitory circuits of the mammalian main olfactory bulb. J Neurophysiol 118:2034-2051.

Chen P, Hong W (2018) Neural Circuit Mechanisms of Social Behavior. Neuron 98:16-30.

Chung HJ, Steinberg JP, Huganir RL, Linden DJ (2003) Requirement of AMPA receptor GluR2 phosphorylation for cerebellar long-term depression. Science 300:1751-1755.

Croy I, Nordin S, Hummel T (2014) Olfactory disorders and quality of life--an updated review. Chem Senses 39:185-194.

Davis HE, McCorkell L, Vogel JM, Topol EJ (2023) Long COVID: major findings, mechanisms and recommendations. Nature Reviews Microbiology 21:133-146.

Del Punta K, Puche A, Adams NC, Rodriguez I, Mombaerts P (2002) A divergent pattern of sensory axonal projections is rendered convergent by second-order neurons in the accessory olfactory bulb. Neuron 35:1057-1066.

Demir E, Li K, Bobrowski-Khoury N, Sanders JI, Beynon RJ, Hurst JL, Kepecs A, Axel R (2020) The pheromone darcin drives a circuit for innate and reinforced behaviours. Nature 578:137-141.

Doty RL (2012) Olfaction in Parkinson's disease and related disorders. Neurobiol Dis 46:527-552.

Doty RL (2017) Olfactory dysfunction in neurodegenerative diseases: is there a common pathological substrate? Lancet Neurol 16:478-488.

Dulac C, Torello AT (2003) Molecular detection of pheromone signals in mammals: from genes to behaviour. Nat Rev Neurosci 4:551-562.

Dulac C, Wagner S (2006) Genetic analysis of brain circuits underlying pheromone signaling. Annu Rev Genet 40:449-467.

Dulac C, Kimchi T (2007) Neural mechanisms underlying sex-specific behaviors in vertebrates. Curr Opin Neurobiol 17:675-683.

Garcia J, Koelling RA (1966) Relation of cue to consequence in avoidance learning. Psychonomic Science 4:123-124.

Gschwend O, Abraham NM, Lagier S, Begnaud F, Rodriguez I, Carleton A (2015) Neuronal pattern separation in the olfactory bulb improves odor discrimination learning. Nat Neurosci 18:1474-+.

Halpern M (1987) The organization and function of the vomeronasal system. Annu Rev Neurosci 10:325-362.

Hayashi Y, Momiyama A, Takahashi T, Ohishi H, Ogawa-Meguro R, Shigemoto R, Mizuno N, Nakanishi S (1993) Role of a metabotropic glutamate receptor in synaptic modulation in the accessory olfactory bulb. Nature 366:687-690.

Hendrickson RC, Krauthamer S, Essenberg JM, Holy TE (2008) Inhibition shapes sex selectivity in the mouse accessory olfactory bulb. J Neurosci 28:12523-12534.

Holy TE (2018) The Accessory Olfactory System: Innately Specialized or Microcosm of Mammalian Circuitry? Annu Rev Neurosci 41:501-525.

Hurst JL, Beynon RJ (2004) Scent wars: the chemobiology of competitive signalling in mice. Bioessays 26:1288-1298.

Isogai Y, Si S, Pont-Lezica L, Tan T, Kapoor V, Murthy VN, Dulac C (2011) Molecular organization of vomeronasal chemoreception. Nature 478:241-245.
Jabarin R, Netser S, Wagner S (2022) Beyond the three-chamber test: toward a multimodal and objective assessment of social behavior in rodents. Mol Autism 13:41.
Kang N, Baum MJ, Cherry JA (2009) A direct main olfactory bulb projection to the 'vomeronasal' amygdala in female mice selectively responds to volatile pheromones from males. Eur J Neurosci 29:624-634.
Karlson P, Luscher M (1959) Pheromones': a new term for a class of biologically active substances. Nature 183:55-56.
Lehman MN, Winans SS, Powers JB (1980) Medial nucleus of the amygdala mediates chemosensory control of male hamster sexual behavior. Science 210:557-560.
Leinders-Zufall T, Cockerham RE, Michalakis S, Biel M, Garbers DL, Reed RR, Zufall F, Munger SD (2007) Contribution of the receptor guanylyl cyclase GC-D to chemosensory function in the olfactory epithelium. Proc Natl Acad Sci U S A 104:14507-14512.
Li Y, Mathis A, Grewe BF, Osterhout JA, Ahanonu B, Schnitzer MJ, Murthy VN, Dulac C (2017) Neuronal Representation of Social Information in the Medial Amygdala of Awake Behaving Mice. Cell 171:1176-1190 e1117.
Liberles SD, Buck LB (2006) A second class of chemosensory receptors in the olfactory epithelium. Nature 442:645-650.
Lundstrom JN, Olsson MJ (2005) Subthreshold amounts of social odorant affect mood, but not behavior, in heterosexual women when tested by a male, but not a female, experimenter. Biol Psychol 70:197-204.
Luo M, Fee MS, Katz LC (2003) Encoding pheromonal signals in the accessory olfactory bulb of behaving mice. Science 299:1196-1201.
Ma M (2010) Multiple Olfactory Subsystems Convey Various Sensory Signals. In: The Neurobiology of Olfaction (Menini A, ed). Boca Raton (FL).
Ma M (2012) Odor and pheromone sensing via chemoreceptors. Adv Exp Med Biol 739:93-106.
Mahajan S, Sen D, Sunil A, Srikanth P, Marathe SD, Shaw K, Sahare M, Galande S, Abraham NM (2023) Knockout of angiotensin converting enzyme-2 receptor leads to morphological aberrations in rodent olfactory centers and dysfunctions associated with sense of smell. Front Neurosci 17:1180868.
Mahajan S, Tamboli S, Das S, Bhattacharjee AS, Pardasani M, Srikanth P, Marathe SD, Adlakha A, Ranjan L, Pandey S, Abraham NM (2024) Mouse olfactory system acts as anemo-detector and -discriminator. bioRxiv:2024.2008.2028.610087.
Maksimova MA, Cansler HL, Zuk KE, Torres JM, Roberts DJ, Meeks JP (2019) Interneuron Functional Diversity in the Mouse Accessory Olfactory Bulb. eNeuro 6.
Mohrhardt J, Nagel M, Fleck D, Ben-Shaul Y, Spehr M (2018) Signal Detection and Coding in the Accessory Olfactory System. Chem Senses 43:667-695.
Mombaerts P (2004) Genes and ligands for odorant, vomeronasal and taste receptors. Nat Rev Neurosci 5:263-278.
Mombaerts P, Wang F, Dulac C, Chao SK, Nemes A, Mendelsohn M, Edmondson J, Axel R (1996) Visualizing an olfactory sensory map. Cell 87:675-686.
Moncho-Bogani J, Martinez-Garcia F, Novejarque A, Lanuza E (2005) Attraction to sexual pheromones and associated odorants in female mice involves activation of the reward system and basolateral amygdala. Eur J Neurosci 21:2186-2198.
Moore JD, Deschenes M, Furuta T, Huber D, Smear MC, Demers M, Kleinfeld D (2013) Hierarchy of orofacial rhythms revealed through whisking and breathing. Nature 497:205-210.
Mori K, Nagao H, Yoshihara Y (1999) The olfactory bulb: coding and processing of odor molecule information. Science 286:711-715.
Mucignat-Caretta C, Redaelli M, Caretta A (2012) One nose, one brain: contribution of the main and accessory olfactory system to chemosensation. Front Neuroanat 6:46.

Murata K, Touhara K (2021) Pheromones in Vertebrates. In: eLS, pp 1-10.
Pandey S, Bapat V, Abraham JN, Abraham NM (2024) Long COVID: From olfactory dysfunctions to viral Parkinsonism. World J Otorhinolaryngol Head Neck Surg 10:137-147.
Pardasani M, Abraham NM (2022) Neurotropic SARS-CoV-2: Causalities and Realities. In: COVID-19 Pandemic, Mental Health and Neuroscience (Sara P, Berend O, eds), p Ch. 1. Rijeka: IntechOpen.
Pardasani M, Marathe SD, Purnapatre MM, Dalvi U, Abraham NM (2021) Multimodal learning of pheromone locations. Faseb J 35.
Pardasani M, Ramakrishnan AM, Mahajan S, Kantroo M, McGowan E, Das S, Srikanth P, Pandey S, Abraham NM (2023) Perceptual learning deficits mediated by somatostatin releasing inhibitory interneurons of olfactory bulb in an early life stress mouse model. Mol Psychiatry.
Ramm SA, Cheetham SA, Hurst JL (2008) Encoding choosiness: female attraction requires prior physical contact with individual male scents in mice. Proc Biol Sci 275:1727-1735.
Ranade S, Hangya B, Kepecs A (2013) Multiple Modes of Phase Locking between Sniffing and Whisking during Active Exploration. Journal of Neuroscience 33:8250-8256.
Rao VR, Pintchovski SA, Chin J, Peebles CL, Mitra S, Finkbeiner S (2006) AMPA receptors regulate transcription of the plasticity-related immediate-early gene Arc. Nat Neurosci 9:887-895.
Rodriguez I, Feinstein P, Mombaerts P (1999) Variable patterns of axonal projections of sensory neurons in the mouse vomeronasal system. Cell 97:199-208.
Salazar I, Sanchez-Quinteiro P, Cifuentes JM, Fernandez De Troconiz P (2006) General organization of the perinatal and adult accessory olfactory bulb in mice. Anat Rec A Discov Mol Cell Evol Biol 288:1009-1025.
Savic I, Berglund H, Gulyas B, Roland P (2001) Smelling of odorous sex hormone-like compounds causes sex-differentiated hypothalamic activations in humans. Neuron 31:661-668.
Schaefer AT, Margrie TW (2007) Spatiotemporal representations in the olfactory system. Trends Neurosci 30:92-100.
Schoppa NE, Urban NN (2003) Dendritic processing within olfactory bulb circuits. Trends Neurosci 26:501-506.
Schwende FJ, Wiesler D, Jorgenson JW, Carmack M, Novotny M (1986) Urinary volatile constituents of the house mouse,Mus musculus, and their endocrine dependency. J Chem Ecol 12:277-296.
Spehr M, Kelliher KR, Li XH, Boehm T, Leinders-Zufall T, Zufall F (2006) Essential role of the main olfactory system in social recognition of major histocompatibility complex peptide ligands. J Neurosci 26:1961-1970.
Stern K, McClintock MK (1998) Regulation of ovulation by human pheromones. Nature 392:177-179.
Steward O, Worley PF (2001) Selective targeting of newly synthesized Arc mRNA to active synapses requires NMDA receptor activation. Neuron 30:227-240.
Taniguchi M, Kaba H (2001) Properties of reciprocal synapses in the mouse accessory olfactory bulb. Neuroscience 108:365-370.
Tirindelli R (2021) Coding of pheromones by vomeronasal receptors. Cell Tissue Res 383:367-386.
Trotier D, Eloit C, Wassef M, Talmain G, Bensimon JL, Doving KB, Ferrand J (2000) The vomeronasal cavity in adult humans. Chem Senses 25:369-380.
Uchida N, Kepecs A, Mainen ZF (2006) Seeing at a glance, smelling in a whiff: rapid forms of perceptual decision making. Nat Rev Neurosci 7:485-491.
Urban NN (2002) Lateral inhibition in the olfactory bulb and in olfaction. Physiol Behav 77:607-612.
Wachowiak M (2011) All in a Sniff: Olfaction as a Model for Active Sensing. Neuron 71:962-973.
Watt AJ, Sjostrom PJ, Hausser M, Nelson SB, Turrigiano GG (2004) A proportional but slower NMDA potentiation follows AMPA potentiation in LTP. Nat Neurosci 7:518-524.
Welker WI (1964) Analysis of Sniffing of the Albino Rat Behaviour 22:223-244.
Wesson DW (2013) Sniffing Behavior Communicates Social Hierarchy. Curr Biol 23:575-580.
Witt M, Georgiewa B, Knecht M, Hummel T (2002) On the chemosensory nature of the vomeronasal epithelium in adult humans. Histochem Cell Biol 117:493-509.

Wyatt TD (2014) Pheromones and Animal Behavior: Chemical Signals and Signatures, 2 Edition. Cambridge: Cambridge University Press.

Acknowledgements

We thank Laboratory of Neural Circuits and Behavior (LNCB) members and IISER-Pune Biology colleagues for fruitful discussions. We thank staff of *National Facility for Gene Function in Health and Disease* (NFGFHD) and IISER Biology- Leica microscopy facility for the technical support. Some of the illustrations were created with BioRender.com.
Funding: This work was supported by the DBT/Wellcome Trust India Alliance senior grant (IA/S/22/2/506517 to N.M.A.), DBT/Wellcome Trust India Alliance intermediate grant (IA/I/14/1/501306 to N.M.A.), DST-Cognitive Science Research Initiative (DST/CSRI/2017/271 to N.M.A.), and CSIR Fellowship (S.D.M.). Part of the work was carried at the National Facility for Gene Function in Health and Disease (NFGFHD) at IISER Pune, supported by a grant from the Department of Biotechnology, Govt. of India (BT/INF/22/SP17358/2016).

Author Contributions

N.M.A. supervised all aspects of the project. N.M.A. carried out the study conceptualization and experimental design. S.D.M. performed all experiments and analysed the data. N.M.A. and S.D.M. wrote the manuscript.

Competing Interests

The authors have stated explicitly that there are no conflicts of interests in connection with this article.

Data and Materials Availability

All cumulative data are available in the article/supplementary materials, further inquiries can be directed to the corresponding author.

List of supplementary material

Supplementary Figures S1 to S3